Symbiotic Radio based Spectrum Sharing in Cooperative UAV-IRS Wireless Networks

Sourabh Solanki*, Sumit Gautam†, Vibhum Singh*, Shree K. Sharma*, and Symeon Chatzinotas*
*Interdisciplinary Centre for Security, Reliability and Trust (SnT), University of Luxembourg, Luxembourg
†Department of Electrical Engineering, Indian Institute of Technology Indore, India,
Email:{sourabh.solanki,vibhum.singh,symeon.chatzinotas}@uni.lu, sumit.gautam@iiti.ac.in, shree.sharma@ieee.org

***Abstract*—Ambient backscatter communication (AmBC) technology can potentially offer spectral- and energy-efficient solutions for future wireless systems. This paper proposes a novel design to facilitate the spectrum sharing between a secondary system and a primary system based on the AmBC technique in intelligent reflective surface (IRS)-assisted unmanned aerial vehicle (UAV) networks. In particular, an IRS-aided UAV cooperatively relays the transmission from a terrestrial primary source node to a user equipment on the ground. On the other hand, leveraging on the AmBC technology, a terrestrial secondary node transmits its information to a terrestrial secondary receiver by modulating and backscattering the ambient relayed radio frequency (RF) signals from the UAV-IRS. The performance of such a system setup is analyzed by deriving the expressions of outage probability and ergodic spectral efficiency. Finally, we present the numerical results to provide useful insights into the system design and also validate the derived theoretical results using Monte Carlo simulations.**

I. Introduction

INTELLIGENT reflective surfaces (IRSs) are envisaged to have a great potential for their applications in the next generation of wireless networks, including the internet-of-things (IoT) networks. The IRSs are comprised of a synthetic array having sub-wavelength passive reflector elements that can adjust the phase shifts of the impinging waves, in order to efficiently steer them towards the destination. In the context of the future 6G wireless networks, the IRSs can offer higher energy- and spectral- efficiency with reduced hardware complexity and cost compared to the traditional cooperative relaying schemes [1]. On another front, unmanned aerial vehicles (UAVs) are believed to play a crucial role in providing wireless connectivity and coverage to the ground users, especially for emergency service or hot-spot. Due to their mobility and high altitude, UAVs can establish their individual direct line-of-sight (LoS) links with the ground users to counteract blockages and shadowing in the complex urban environment [2], [3].

Ambient backscatter communication (AmBC) is another technology that can utilize the radio-frequency (RF) signals from the ambient base stations, TV towers, or access points, for the transmission without requiring active RF components [4], [5]. Communication using AmBC does not require a dedicated spectrum and thus, offers spectral efficient means for wireless information transmission. Leveraging on the potential of AmBC, authors in [6] introduced a spectrum sharing paradigm for IoT devices. Authors in [7] studied a cognitive backscatter network based spectrum sharing for passive IoT. Moreover, a symbiotic radio cooperative AmBC has been analyzed in [8] to facilitate the spectrum sharing. Recently, authors in [9] examined the outage performance in three different paradigms of cooperative AmBC systems.

Motivated by the above-mentioned discussion and potential of IRS, UAV, and AmBC technologies, we propose a novel system design in this paper wherein an IRS-capable UAV helps a transmit node to relay its information to the destination. Meanwhile, a secondary system co-exists on the same spectrum relying on the AmBC assistance. The UAV-IRS methodology can provide a wide coverage in ultra-dense environments, whereas, the employment of AmBC augments in the effective usage of spectral resources.

In contrast to cognitive radio based spectrum sharing [10], the co-existence using AmBC primarily differs in two aspects. First, the secondary transmitter (Tag) does not generate its own RF signal but exploits the RF signal of primary transmitter for its information transmission. Second, due to interference from the primary system, the secondary receiver (Reader) relies upon the successive interference cancellation (SIC) to decode its information. This spectrum sharing concept has also been referred to as a symbiotic radio or cognitive backscattering [11]. For such a system configuration, we comprehensively investigate its performance by deriving theoretical expressions for the outage probability (OP) and ergodic spectral efficiency (ESE). Based on our investigations, we provide various insights into the system design.

Notations: We use $\mathbb{E}[\cdot]$ to represent the expectation and $\mathcal{CN}(0,\sigma^2)$ to represent complex normal distribution having mean zero and variance σ^2. $\mathbf{I}_N$ denotes the identity matrix of size $N \times N$, $K_v(\cdot)$ represents v-th order modified Bessel function of second kind [12, eq. (8.432.1)], whereas $\mathcal{W}_{u,v}(\cdot)$ denotes Whittaker function [12, eq. (9.222)]. $f_X(\cdot)$ and $F_X(\cdot)$ denote the probability density function (PDF) and the cumulative distribution function (CDF) of a random variable (RV) X, respectively, and $\Pr[\cdot]$ represents the probability. $\Upsilon[\cdot,\cdot]$ and $\Gamma[\cdot]$ denote, respectively, the lower incomplete and the complete gamma functions [12, eq. (8.350)].

II. System Model

We consider a wireless network comprising a primary system including a transmit node S, a UAV-IRS [13], and a UE on the ground. The secondary system includes a backscatter capable transmitter T and a receiver R. The system operates in sub-6GHz band [14]. Hereby, we assume the cooperation between primary and secondary systems to facilitate the joint decoding at R, which, in turn, can achieve a reliable backscatter communication [8], [9]. Due to the absence of an LoS

link, S relays its information via assistance from an UAV-IRS with N passive reflective elements that can be reconfigured using a controller. Such a network configuration may be useful to offload the cell traffic using the aerial nodes to serve the cell-edge users which are beyond the strong coverage of base station in a macrocell. Location of S, UAV, and ground users are denoted by $\{\mathbf{q_b}, \mathbf{q_u}, \mathbf{q_k}\} \in \mathbb{R}^{3\times 1}$ with $\mathbf{k} \in \{\mathbf{e}, \mathbf{t}, \mathbf{r}\}$, respectively, in a three-dimensional plane. The UAV is assumed to be a fixed-wing type which follows a circular trajectory of radius r at a fixed altitude $H \in [H_{\min}, H_{\max}]$ with a constant velocity, where $H_{\min}$ and $H_{\max}$ being the minimum and maximum possible altitudes. Let us consider θ as an angle of the UAV location with reference to x-axis at any given instant. Thus, UAV's location can be represented as $\mathbf{q_u} = [r\cos\theta \quad r\sin\theta \quad H]^T$.

As such, the elevation angle between S and UAV, denoted as $\phi_{\mathbf{b,u}}$, and between ground users and UAV, denoted as $\phi_{\mathbf{k,u}}$, can be expressed as

$$\phi_{\mathbf{b,u}} = \arctan\left(\frac{H}{|\mathbf{q_u} - \mathbf{q_b}|}\right), \; \phi_{\mathbf{k,u}} = \arctan\left(\frac{H}{|\mathbf{q_u} - \mathbf{q_k}|}\right). \quad (1)$$

The LoS probability between UAV and ground nodes i.e., S and UEs, is given by [15]

$$p^L(\phi_{\ell,\mathbf{u}}) = \frac{1}{1 + C\exp\left(-B(\phi_{\ell,\mathbf{u}} - C)\right)}, \quad \forall \ell \in \{\mathbf{b}, \mathbf{k}\} \quad (2)$$

where B and C are environment dependent constants. The path-loss exponent is given by $\alpha(\phi_{\ell,\mathbf{u}}) = p^L(\phi_{\ell,\mathbf{u}})c_\ell + f_\ell$ where c_ℓ and f_ℓ are constants which depend on the uplink and downlink environment. The channels from S to n-th IRS element at UAV and from n-th IRS element to UE and R, are denoted, respectively, as $h_{b,n}$, $h_{n,e}$ and $h_{n,r}$. The composite channels from n-th IRS element to R and UE via T are represented by h_{n,t_r} and h_{n,t_e}, respectively [7]-[9]. All the channels are assumed to follow uncorrelated quasi-static Rayleigh fading such that $\mathbf{h}_{u,\kappa} \sim \mathcal{CN}(0, \Omega_{u\kappa}\mathbf{I}_N)$ with $\kappa \in \{e, r, t_e, t_r\}$. Further, we can represent $\mathbf{h}_{b,u} = [h_{b,1}, \cdots, h_{b,N}]^H$, $\mathbf{h}_{u,e} = [h_{1,e}, \cdots, h_{N,e}]^H$, $\mathbf{h}_{u,r} = [h_{1,r}, \cdots, h_{N,r}]^H$, $\mathbf{h}_{u,t_e} = [h_{1,t_e}, \cdots, h_{N,t_e}]^H$, and $\mathbf{h}_{u,t_r} = [h_{1,t_r}, \cdots, h_{N,t_r}]^H$. $\mathbf{\Theta} = \text{diag}(e^{j\varphi_1}, \cdots, e^{j\varphi_n}, \cdots, e^{j\varphi_N})$ is a phase shift matrix, where $\varphi_n \in [0, 2\pi), \forall n$, is the phase shift by the n-th element.

III. Modeling of IRS-Aided UAV Networks

A. SNR Formulation

First, S transmits its symbol x with $\mathbb{E}[x^2] = 1$ to UE via assistance from the UAV-IRS. Meanwhile, the secondary node T modulates its own information c with $\mathbb{E}[c^2] = 1$, on the received RF signal from UAV-IRS, to transmit for its destination R. As a result, the signal received at UE can be given as

$$y_e = \sqrt{P_b\tilde{d}_1}\mathbf{h}_{b,u}^H\mathbf{\Theta}\mathbf{h}_{u,e}x + \sqrt{P_b\eta\tilde{d}_2}\mathbf{h}_{b,u}^H\mathbf{\Theta}\mathbf{h}_{u,t_e}xc + \nu_e, \quad (3)$$

where P_b is the transmit power at the S, $\tilde{d}_1 = d_{bu}^{-\alpha(\phi_{\mathbf{b,u}})}d_{ue}^{-\alpha(\phi_{\mathbf{u,e}})}$, $\tilde{d}_2 = d_{bu}^{-\alpha(\phi_{\mathbf{b,u}})}d_{ut}^{-\alpha(\phi_{\mathbf{u,t}})}d_{te}^{-\alpha_o}$, with $d_{bu} = \sqrt{|\mathbf{q}_b - \mathbf{q}_u|^2 + H^2}$, $d_{ue} = \sqrt{|\mathbf{q_e} - \mathbf{q}_u|^2 + H^2}$, $d_{ut} = \sqrt{|\mathbf{q_t} - \mathbf{q}_u|^2 + H^2}$, and $d_{te} = |\mathbf{q_t} - \mathbf{q_e}|$, being the distances between S to UAV-IRS, UAV-IRS to UE, and T to UE, respectively. α_o is the path-loss exponent for the terrestrial links, $\eta \in [0, 1]$ is the backscatter efficiency of T, and $\nu_e \sim \mathcal{CN}(0, \sigma_e^2)$ is the additive white Gaussian noise (AWGN). On the other hand, the signal received at R is given by

$$y_r = \sqrt{P_b\eta\tilde{d}_3}\mathbf{h}_{b,u}^H\mathbf{\Theta}\mathbf{h}_{u,t_r}xc + \sqrt{P_b\tilde{d}_4}\mathbf{h}_{b,u}^H\mathbf{\Theta}\mathbf{h}_{u,r}x + \nu_r, \quad (4)$$

where $\tilde{d}_3 = d_{bu}^{-\alpha(\phi_{\mathbf{b,u}})}d_{ut}^{-\alpha(\phi_{\mathbf{u,t}})}d_{tr}^{-\alpha_o}$, $\tilde{d}_4 = d_{bu}^{-\alpha(\phi_{\mathbf{b,u}})}d_{ur}^{-\alpha(\phi_{\mathbf{u,r}})}$, with $d_{ur} = \sqrt{|\mathbf{q_r} - \mathbf{q}_u|^2 + H^2}$, and $d_{tr} = |\mathbf{q_t} - \mathbf{q_r}|$ being the distances between UAV-IRS to R, and T to R, respectively, and $\nu_r \sim \mathcal{CN}(0, \sigma_r^2)$ is the AWGN. As highlighted earlier, due to cooperation between primary and secondary systems, node R can decode its information c using SIC [7]-[9]. Specifically, it first decodes the signal of UE while treating c as an interference and subsequently obtains its information by eliminating the decoded signal. As such, the signal-to-interference-plus-noise ratio (SINR) at R to decode the x can be given by

$$\Lambda_R^x = \frac{P_b\tilde{d}_4\left|\mathbf{h}_{b,u}^H\mathbf{\Theta}\mathbf{h}_{u,r}\right|^2}{P_b\eta\tilde{d}_3\left|\mathbf{h}_{b,u}^H\mathbf{\Theta}\mathbf{h}_{u,t_r}\right|^2 + \sigma_r^2}. \quad (5)$$

After eliminating the decoded signal x from its observation, R retrieves its information using the SNR

$$\Lambda_R^c = \frac{P_b}{\sigma_r^2}\eta\tilde{d}_3\left|\mathbf{h}_{b,u}^H\mathbf{\Theta}\mathbf{h}_{u,t_r}\right|^2, \quad (6)$$

whereas, the UE decodes its information using the SINR as

$$\Lambda_E^x = \frac{P_b\tilde{d}_1\left|\mathbf{h}_{b,u}^H\mathbf{\Theta}\mathbf{h}_{u,e}\right|^2}{P_b\eta\tilde{d}_2\left|\mathbf{h}_{b,u}^H\mathbf{\Theta}\mathbf{h}_{u,t_e}\right|^2 + \sigma_e^2}. \quad (7)$$

Hereby, we consider a coherent phase shift design [16] to maximize the performance of primary user UE. In other words, we assume that the phase shifts from the IRS elements are adjusted in such a way that the reflected signals are co-phased, i.e., $\varphi_n = \arg h_{b,n}h_{n,e}$. It is assumed that the channel state information (CSI) of the pertinent channels are available at the S which can be feedback to IRS controller from a dedicated control channel. Various methods of the channel estimation have been reported in existing works, for instance, see [17]. Note that as IRS configures itself to optimize the phase shifts for UE, nodes T and R will experience the arbitrary phase shifts. For notational simplicity, let us represent $X = \mathbf{h}_{b,u}^H\mathbf{\Theta}\mathbf{h}_{u,e} = \sum_{n=1}^N |h_{b,n}||h_{n,e}|$, $W = |\mathbf{h}_{b,u}^H\mathbf{\Theta}\mathbf{h}_{u,t_e}|^2$, $Y = |\mathbf{h}_{b,u}^H\mathbf{\Theta}\mathbf{h}_{u,r}|^2$, and $Z = |\mathbf{h}_{b,u}^H\mathbf{\Theta}\mathbf{h}_{u,t_r}|^2$.

B. Probability of Successful SIC

Recalling that node R first needs to decode the information of UE to extract its own information. We define this requirement for node R as the condition of successful SIC and obtain its probability as

$$\begin{aligned} P_{sic}(\tau) &= \Pr[\Lambda_R^x > \tau] \\ &= 1 - \Pr\left[\frac{P_b\tilde{d}_4\left|\mathbf{h}_{b,u}^H\mathbf{\Theta}\mathbf{h}_{u,r}\right|^2}{P_b\eta\tilde{d}_3\left|\mathbf{h}_{b,u}^H\mathbf{\Theta}\mathbf{h}_{u,t_r}\right|^2 + \sigma_r^2} \le \tau\right] \\ &= 1 - \int_{z=0}^{\infty} F_Y\left(\frac{\tau}{P_b\tilde{d}_4}(P_b\eta\tilde{d}_3 z + \sigma_r^2)\right) f_Z(z)dz, \end{aligned} \quad (8)$$

where τ is the minimum required threshold to decode the information.

Theorem 1. *The probability of successful SIC at R is given by*

$$P_{sic}(\tau) = 1 - \sum_{m=0}^{L} \frac{\mathcal{A}(\tau)\Gamma(k_y)\Gamma(k_z)}{\Gamma(k_y+m+1)} \left(1+\frac{\tilde{d}_4\beta_y}{\tau\eta\tilde{d}_3\beta_z}\right)^{-\frac{\zeta}{2}} \times \left(\frac{\tau\sigma_r^2}{P_b\tilde{d}_4\beta_y}\right)^{\frac{\zeta}{2}-1} \exp\left(\frac{-\tau\sigma_r^2}{2P_b\tilde{d}_4\beta_y}\left(1+\frac{\tilde{d}_4\beta_y}{\tau\eta\tilde{d}_3\beta_z}\right)\right) \times \mathcal{W}_{\frac{\zeta-2k_z}{2},\frac{1-\zeta}{2}}\left(\left(1+\frac{\tilde{d}_4\beta_y}{\tau\eta\tilde{d}_3\beta_z}\right)\frac{\tau\sigma_r^2}{2P_b\tilde{d}_4\beta_y}\right), \quad (9)$$

where $k_y = k_z = N/(N+2), \beta_y = \Omega_{bu}\Omega_{ur}(N+2), \beta_z = \Omega_{bu}\Omega_{ut_r}(N+2), \zeta = k_y + k_z + m + 1.$

Proof. Please refer to Appendix A. ■

The result of Theorem 1 will be utilized to analyze the performance of secondary system in the subsequent section.

IV. Performance Analysis of the Proposed AmBC Assisted Co-existence

This section analyzes the performance of the considered framework by evaluating two key metrics e.g., OP and ESE.

A. Outage Probability

1) Primary System: The primary system is said to be in outage [18] if the received SINR at UE, i.e., Λ_E^x, falls below a certain threshold. For a given target rate $\mathcal{R}_p$, OP can be expressed as

$$P_{out}^{pri}(\mathcal{R}_p) = \Pr\left[\frac{P_b\tilde{d}_1\left|\sum_{n=1}^{N} h_{b,n}e^{j\varphi_n}h_{n,e}\right|^2}{P_b\eta\tilde{d}_2\left|\mathbf{h}_{b,u}^H\mathbf{\Theta}\mathbf{h}_{u,t_e}\right|^2+\sigma_e^2} \le r_{th}^p\right], \quad (10)$$

where $r_{th}^p = 2^{\mathcal{R}_p} - 1$. In the following theorem, we provide the closed-form expression for the OP.

Theorem 2. *The OP of primary system is given by*

$$P_{out}^{pri}(\mathcal{R}_p) = \mathcal{B}(l,n)\Gamma(k_w)\left(\frac{\tilde{d}_1\beta_x^2}{r_{th}^p\eta\tilde{d}_2\beta_w}\right)^{-\frac{\xi+2}{4}}\left(\frac{r_{th}^p\sigma_e^2}{P_b\tilde{d}_1\beta_x^2}\right)^{\frac{\xi-2}{4}} \times \exp\left(\frac{-\sigma_e^2}{2\eta\tilde{d}_2\beta_w P_b}\right)\mathcal{W}_{\frac{\xi-4k_w}{4},\frac{-\xi}{4}}\left(\frac{\sigma_e^2}{\eta\tilde{d}_2\beta_w P_b}\right), \quad (11)$$

where $\xi = k_x + 2k_w + l + n.$

Proof. Please refer to Appendix B. ■

2) Backscattering Secondary System: In the backscattering secondary system, an outage occurs if either R is unable to successfully perform SIC or SNR at R i.e., Λ_R^c, falls below a specific threshold. Based on the SIC probability, the OP can be formulated as

$$P_{out}^{sec}(\mathcal{R}_s) = \bar{P}_{sic}(\tau) + P_{sic}(\tau)\Pr[\log_2(1+\Lambda_R^c) \le \mathcal{R}_s] = \bar{P}_{sic}(\tau) + P_{sic}(\tau)\Pr\left[\frac{P_b}{\sigma_r^2}\eta\tilde{d}_3\left|\mathbf{h}_{b,u}^H\mathbf{\Theta}\mathbf{h}_{u,t_r}\right|^2 \le r_{th}^s\right], \quad (12)$$

where $\mathcal{R}_s$ is a target rate and $r_{th}^s = 2^{\mathcal{R}_s} - 1$ and $P_{sic}(\tau)$ is as given in Theorem 1, with $\bar{P}_{sic}(\tau) = 1 - P_{sic}(\tau)$. Following corollary provides the closed-form solution for the above equation.

Corollary 1. *The OP of the backscattering secondary system can be expressed as*

$$P_{out}^{sec}(\mathcal{R}_s) = \bar{P}_{sic}(\tau) + P_{sic}(\tau)\frac{1}{\Gamma(k_z)}\Upsilon\left(k_z, \frac{r_{th}^{s,ct}\sigma_r^2}{P_b\eta\tilde{d}_3\beta_z}\right), \quad (13)$$

Proof. Using the statistical properties of $Z = |\mathbf{h}_{b,u}^H\mathbf{\Theta}\mathbf{h}_{u,t_r}|^2$ in Appendix A, RV Z follows Gamma distribution with CDF $F_Z(z) = \frac{1}{\Gamma(k_z)}\Upsilon(k_z, z/\beta_z)$. Based on this CDF, we can obtain the desired expression in Corollary 1. ■

B. Ergodic Spectral Efficiency

1) Primary System: For the primary system, the ESE can be expressed as

$$C_{pri} = \mathbb{E}\left[\log_2\left(1+\frac{P_b\tilde{d}_1\left|\sum_{n=1}^{N} h_{b,n}e^{j\varphi_n}h_{n,e}\right|^2}{P_b\eta\tilde{d}_2\left|\mathbf{h}_{b,u}^H\mathbf{\Theta}\mathbf{h}_{u,t_e}\right|^2+\sigma_e^2}\right)\right] = \mathbb{E}\left[\log_2\left(P_b\tilde{d}_1X^2 + P_b\eta\tilde{d}_2W + \sigma_e^2\right)\right] - \mathbb{E}\left[\log_2\left(P_b\eta\tilde{d}_2W + \sigma_e^2\right)\right]. \quad (14)$$

It appears that obtaining the closed-form solution of the above expression is rather intricate due to underlying statistical dependence between the two terms. Therefore, we seek for its approximation by using the Jensen's inequality, as follows

$$C_{pri} \approx \log_2\left(P_b\tilde{d}_1\mathbb{E}[X^2] + P_b\eta\tilde{d}_2\mathbb{E}[W] + \sigma_e^2\right) - \log_2\left(P_b\eta\tilde{d}_2\mathbb{E}[W] + \sigma_e^2\right), \quad (15)$$

following the statistical characterization in Appendix B, one can obtain $\mathbb{E}[W] = k_w\beta_w$ and $\mathbb{E}[X^2] = k_x\beta_x^2(1+k_x)$. Finally, using these values in (15), we can obtain a simplified approximation for the ESE of primary system.

2) Backscattering Secondary System: For the secondary system, the ESE can be expressed as

$$C_{sec} = P_{sic}(\tau)\mathbb{E}\left[\log_2\left(1+\frac{P_b}{\sigma_r^2}\eta\tilde{d}_3\left|\mathbf{h}_{b,u}^H\mathbf{\Theta}\mathbf{h}_{u,t_r}\right|^2\right)\right] = P_{sic}(\tau)\int_0^\infty \log_2\left(1+\frac{P_b}{\sigma_r^2}\eta\tilde{d}_3 z\right)f_Z(z)dz, \quad (16)$$

after some manipulations followed by invoking Meijer G-function representation $\Gamma(q,t) = G_{1,2}^{2,0}\left(t\middle|\begin{smallmatrix}1\\1,q\end{smallmatrix}\right)$, (16) can be expressed as

$$C_{sec} = \frac{P_{sic}(\tau)}{\Gamma(k_z)\ln 2}G_{2,3}^{3,1}\left(\frac{\sigma_r^2}{P_b\eta\tilde{d}_3\beta_z}\middle|\begin{matrix}0,1\\0,0,k_z\end{matrix}\right). \quad (17)$$

Using Jensen's inequality, C_{sec} can be simply bounded as $C_{sec} \le \log_2\left(1+\frac{P_b}{\sigma_r^2}\eta\tilde{d}_3k_z\beta_z\right)$.

V. Numerical Results and Discussion

This section presents the numerical results based on the theoretical analysis. Monte Carlo simulations validate the derived results. We set the several system parameters as $\Omega_{bu} = \Omega_{ue} = \Omega_{ur} = 2$, $\Omega_{ut_e} = \Omega_{ut_r} = 0.5$, $C = 20$, $B = 0.5$, $c_\ell = -1.5$, $f_\ell = 3.5$ [15]. For demonstration, without losing generality,

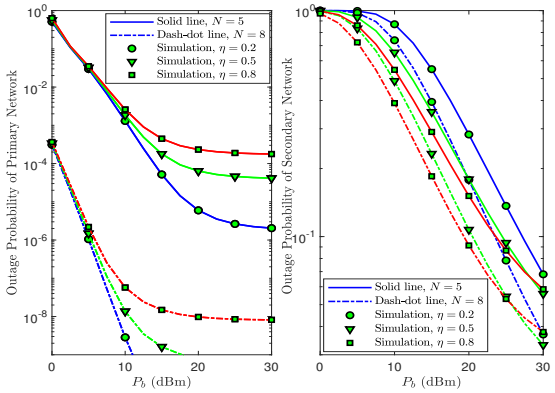

Fig. 1: OP in terms of the transmit power P_b.

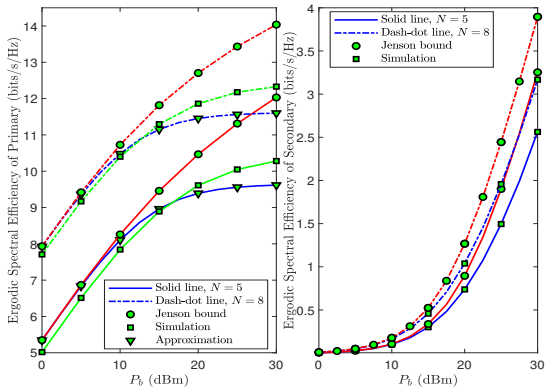

Fig. 2: ESE in terms of the transmit power P_b.

we consider $H = 1.5$ km, $r = 0.5$ km, $R_p = 3, R_s = 0.1$, $\mathbf{q_b} = [-2\ \ -2\ 0]^T$ km, $\mathbf{q_e} = [3\ 0\ 0]^T$ km, $\mathbf{q_t} = [3\ \ -1\ 0]^T$ m, $\mathbf{q_r} = [5\ \ -1\ 0]^T$ m, $\alpha_o = 2.5$, $\tau = 0.1$, $\sigma_e = \sigma_r = 10$ dBm, unless stated otherwise.

In Fig. 1, we plot the outage performance of primary and secondary systems in terms of the transmit power. Apparently, the analytical results are well-matched with the simulation results, which corroborate the theoretical analysis. It can be observed from the curves that as N increases, the performance improves. Nevertheless, the performance of primary is observed to be saturated at high power regime which can be attributed to the interference from the backscattering transmission. Further, as backscattering efficiency η increases, the performance of primary deteriorates while performance of secondary improves. This is associated with the fact that a higher η causes high interference to primary, whereas, it provides additional power for the backscattered transmission. Interestingly, the secondary performance also degrades at high η due to an increased likelihood of SIC failure, as observed in the curves corresponding to $\eta = 0.8$ at 30 dB.

Fig. 2 illustrates the ESE performance. Firstly, it can be noted that the approximation for the primary is fairly close to the simulation results. Further, we note from the pertinent curves that the ESE of both primary and secondary networks can be improved by increasing N. Such performance enhancement with respect to N becomes predominantly significant at higher P_b. However, due to the interference from the backscattered transmission, the ESE of primary tends to saturate in the high transmit power regime.

VI. Conclusion

We investigated a symbiotic radio based spectrum sharing network that enabled AmBC assisted co-existence of a secondary system in UAV-IRS networks. The performance is characterized by analyzing the OP and ESE. Evidently, the deployment of an UAV-IRS leads to enhanced performance for both primary and backscattering secondary systems with respect to reflective elements N. It has been witnessed that backscatter efficiency is a crucial design parameter which can significantly affect the performance of both the systems. Moreover, it is also noted that ESE can be improved by increasing the reflective elements of IRS. In essence, the study demonstrated the viability of co-existence of secondary system in the primary's spectrum using AmBC technology, that can offer both spectral- and energy-efficient solutions for the future wireless networks.

Appendix A
Proof of Theorem 1

To evaluate the integral in (8), we first obtain the CDF of RV Y by following a moment matching method. To proceed, we first write the mean of Y as

$$\mathbb{E}[Y] = \mathbb{E}\left[|\mathbf{h}_{b,u}^H \boldsymbol{\Theta} \mathbf{h}_{u,r}|^2\right] = N\Omega_{bu}\Omega_{ur}. \tag{A.1}$$

Further, we obtain

$$\begin{aligned}\mathbb{E}[Y^2] &= \mathbb{E}\left[|\mathbf{h}_{b,u}^H \boldsymbol{\Theta} \mathbf{h}_{u,r}|^4\right] \\ &= \mathbb{E}\left[||\boldsymbol{\Theta}\mathbf{h}_{u,r}||^4 \left|\frac{\mathbf{h}_{b,u}^H \boldsymbol{\Theta} \mathbf{h}_{u,r}}{||\boldsymbol{\Theta}\mathbf{h}_{u,r}||} \frac{\mathbf{h}_{b,u}^H \boldsymbol{\Theta} \mathbf{h}_{u,r}}{||\boldsymbol{\Theta}\mathbf{h}_{u,r}||}\right|^2\right],\end{aligned} \tag{A.2}$$

by defining $w = \frac{\mathbf{h}_{b,u}^H \boldsymbol{\Theta} \mathbf{h}_{u,r}}{||\boldsymbol{\Theta}\mathbf{h}_{u,r}||}$, we can write $z \sim \mathcal{CN}(0, \Omega_{bu})$ such that [19] $\mathbb{E}[Y^2] = 2N(N+1)\Omega_{bu}^2\Omega_{ur}^2$. Using the above derived statistics, we can obtain variance of Y as $\text{Var[Y]} = \mathbb{E}[Y^2] - (\mathbb{E}[Y])^2 = N(N+2)\Omega_{bu}^2\Omega_{ur}^2$. Finally we can match the distribution of Y to a Gamma distribution with shape k_y and scale β_y parameters as $k_y = (\mathbb{E}[Y])^2/\text{Var[Y]}, \beta_y = \text{Var[Y]}/\mathbb{E}[Y]$. Based on these parameters, we have CDF $F_Y(y) = \frac{1}{\Gamma(k_y)}\Upsilon(k_y, y/\beta_y)$. In a similar way, we can obtain CDF of Z and subsequently its PDF as $f_Z(z) = \frac{1}{\Gamma(k_z)\beta_z^{k_z}} z^{k_z-1}\exp(-z/\beta_z)$. Utilizing $F_Y(y)$ and $f_Z(z)$ in (8), we can write $\bar{P}_{sic}(\tau) = 1 - P_{sic}(\tau)$ as

$$\begin{aligned}\bar{P}_{sic}(\tau) &= \frac{1}{\Gamma(k_y)\Gamma(k_z)\beta_z^{k_z}} \int_0^\infty \Upsilon\left(k_y, \frac{\tau}{P_b\tilde{d}_4}(P_b\eta\tilde{d}_3 z + \sigma_r^2)\right) \\ &\quad \times z^{k_z-1}\exp\left(\frac{-z}{\beta_z}\right) dz \\ &\overset{(a)}{=} \frac{1}{\Gamma(k_y)\Gamma(k_z)\beta_z^{k_z}} \left(\frac{\tilde{d}_4\beta_y}{\tau\eta\tilde{d}_3}\right)^{k_z} \exp\left(\frac{\sigma_r^2}{\beta_z P_b\eta\tilde{d}_3}\right) \int_{t=\frac{\tau\sigma_r^2}{P_b\tilde{d}_4\beta_y}}^\infty \\ &\quad \times \Upsilon(k_y, t)\left(t - \frac{\tau\sigma_r^2}{P_b\tilde{d}_4\beta_y}\right)^{k_z-1} \exp\left(-\frac{t\tilde{d}_4\beta_y}{P_b\eta\tilde{d}_3\beta_z}\right) dt,\end{aligned} \tag{A.3}$$

where (a) is obtained using appropriate substitution. For simplification, let us denote the terms before the integral in (A.3) by $\mathcal{A}(\tau)$. Using the series representation of the lower incomplete gamma function, (A.3) can be re-expressed as

$$\bar{P}_{sic}(\tau)=\sum_{m=0}^{L}\frac{\mathcal{A}(\tau)\Gamma(k_y)}{\Gamma(k_y+m+1)}\int_{\frac{\tau\sigma_r^2}{P_b\tilde{d}_4\beta_y}}^{\infty}t^{k_y+m}\left(t-\frac{\tau\sigma_r^2}{P_b\tilde{d}_4\beta_y}\right)^{k_z-1}\times\exp\left(-t-\frac{t\tilde{d}_4\beta_y}{\tau\eta\tilde{d}_3\beta_z}\right)dt, \tag{A.4}$$

on evaluating the above integral using [12, 3.383.4], one can arrive at the expression in Theorem 2. In (A.4), L equals infinity provides exact values of $\bar{P}_{sic}(\tau)$, however, even for a smaller number $L = 10$, the series converges to sufficient level of accuracy.

Appendix B
Proof of Theorem 2

From (10), we have

$$P_{out}^{pri}(\mathcal{R}_p)=\Pr\left[\frac{P_b\tilde{d}_1X^2}{P_b\eta\tilde{d}_2W+\sigma_e^2}\leq r_{th}^p\right]=\int_{w=0}^{\infty}F_X\left(\sqrt{\frac{r_{th}^p(P_b\eta\tilde{d}_2w+\sigma_e^2)}{P_b\tilde{d}_1}}\right)f_W(w)dw. \tag{B.1}$$

We first characterize the distribution of RV X using moment matching. As $h_{b,n}$ and $h_{n,e}$ follow Rayleigh distribution, the CDF of their product ($\Xi_n = |h_{b,n}||h_{n,e}|$) can be obtained as $F_{\Xi_n}(x) = 1 - \frac{2x}{\sqrt{\Omega_{bu}\Omega_{ue}}}K_1\left(\frac{2x}{\sqrt{\Omega_{bu}\Omega_{ue}}}\right)$. Subsequently, its PDF can be obtained by differentiating the CDF as $f_{\Xi_n}(x) = dF_{\Xi_n}(x)/dx$ using [12, 8.486.11]. As a result, the statistics of Ξ_n based on its PDF can be given by $\mathbb{E}[\Xi_n] = \pi\sqrt{\Omega_{bu}\Omega_{ue}}/4$ and $\mathrm{Var}[\Xi_n] = (1-\pi^2/16)\Omega_{bu}\Omega_{ue}$. Finally, we can match the distribution of X to a Gamma distribution with shape k_x and scale β_x parameters as $k_x = \frac{(\mathbb{E}[X])^2}{\mathrm{Var[X]}} = N\pi^2/(16-\pi^2)$, $\beta_x = \frac{\mathrm{Var[X]}}{\mathbb{E}[X]} = \frac{N}{4\pi}(16-\pi^2)\sqrt{\Omega_{bu}\Omega_{ue}}$. Based on these parameters, the CDF of X is given as $F_X(x) = \frac{1}{\Gamma(k_x)}\Upsilon\left(k_x, x/\beta_x\right)$. Further, following the approach in Appendix A, we obtain PDF of W as $f_W(w) = \frac{1}{\Gamma(k_w)\beta_w^{k_w}}w^{k_w-1}\exp\left(-\frac{w}{\beta_w}\right)$, where $k_w = N/(N+2), \beta_w = \Omega_{bu}\Omega_{ut_e}(N+2)$. On substituting these CDF and PDF in (B.1) and thereby utilizing the series expansions of lower incomplete gamma function and exponential term, we have

$$P_{out}^{pri}(\mathcal{R}_p)=\frac{1}{\Gamma(k_w)\beta_w^{k_w}}\left(\frac{\tilde{d}_1\beta_x^2}{r_{th}^p\eta\tilde{d}_2}\right)^{k_w}\exp\left(\frac{\sigma_e^2}{P_b\beta_w\eta\tilde{d}_2}\right)\times\sum_{l=0}^{L}\sum_{n=0}^{L}\frac{(-1)^n}{n!\Gamma(k_x+l+1)}\int_{v=\frac{r_{th}^p\sigma_e^2}{P_b\tilde{d}_1\beta_x^2}}^{\infty}v^{\frac{k_x+l+n}{2}}\times\left(v-\frac{r_{th}^p\sigma_e^2}{P_b\tilde{d}_1\beta_x^2}\right)^{k_w-1}\exp\left(-\frac{v\tilde{d}_1\beta_x^2}{r_{th}^p\eta\tilde{d}_2\beta_w}\right)dv. \tag{B.2}$$

For simplification, we denote the terms before the integral in (B.2) by $\mathcal{B}(l, n)$. After evaluating the integral in (B.2), the expression in Theorem 2 is obtained.

Acknowledgment

This work was supported by the Luxembourg National Research Fund (FNR)-5G-Sky Project, ref. 13713801, and the SMC funded Micro5G project.

References

[1] M. Di Renzo *et al.* "Reconfigurable intelligent surfaces vs. relaying: Differences, similarities, and performance comparison," *IEEE Open J. Commun. Soc.*, vol. 1, pp. 798-807, Jul. 2020.

[2] M. M. Azari *et al.*, "Evolution of non-terrestrial networks from 5G to 6G: A survey,"*arXiv preprint arXiv:2107.06881*, July. 2021.

[3] M. M. Azari, S. Solanki, S. Chatzinotas, and M. Bennis, "THz-empowered UAVs in 6G: Opportunities, challenges, and trade-offs,"*arXiv preprint arXiv:2201.07886*, Jan. 2022.

[4] N. V. Huynh, D. T. Hoang, X. Lu, D. Niyato, P. Wang, and D. I. Kim, "Ambient backscatter communications: A contemporary survey," *IEEE Commun. Surveys Tuts.*, vol. 20, no. 4, pp. 2889-2922, May 2018.

[5] S. Gautam, S. Solanki, S. K. Sharma, S. Chatzinotas, and B. Ottersten, "Hybrid active-and-passive relaying model for 6G-IoT greencom networks with SWIPT," *Sensors,* vol. 21, no. 18, p. 6013, Sep. 2021.

[6] X. Kang, Y.-C. Liang, and J. Yang, "Riding on the primary: A new spectrum sharing paradigm for wireless-powered IoT devices," *IEEE Trans. Wireless Commun.*, vol. 17, no. 9, pp. 6335-6347, Sep. 2018.

[7] H. Guo, R. Long, and Y.-C. Liang, "Cognitive backscatter network: A spectrum sharing paradigm for passive IoT," *IEEE Commun. Lett.*, vol. 8, no. 5, pp. 1423-1426, Oct. 2019.

[8] H. Guo, Y.-C. Liang, R. Long, and Q. Zhang "Cooperative ambient backscatter system: A symbiotic paradigm for passive IoT," *IEEE Wireless Commun. Lett.*, vol. 8, no. 4, pp. 1191-1194, Aug. 2019.

[9] H. Ding, D. B. da Costa, and J. Ge, "Outage analysis for cooperative ambient backscatter systems," *IEEE Wireless Commun. Lett.*, vol. 9, no. 5, pp. 601-605, May 2020.

[10] S. Solanki *et al.*, "Performance analysis of cognitive relay networks with RF hardware impairments and CEEs in the presence of primary users' interference," *IEEE Trans. Cogn. Commun. Netw.*, vol. 4, no. 2, pp. 406-421, June 2018.

[11] H. Chen, G. Yang, and Y.-C. Liang, "Joint active and passive beamforming for reconfigurable intelligent surface enhanced symbiotic radio system," *IEEE Wireless Commun. Lett.*, vol. 10, no. 5, pp. 1056-1060, May 2021.

[12] I. S. Gradshteyn and I. M. Ryzhik, *Tables of Integrals, Series and Products*, 7th ed., New York, USA, Academic, 2007.

[13] T. Shafique, H. Tabassum, and E. Hossain, "Optimization of wireless relaying with flexible UAV-borne reflecting surfaces," *IEEE Trans. Commun.*, vol. 69, no. 1, pp. 309-325, Jan. 2021.

[14] Q. Tao, J. Wang, and C. Zhong, "Performance analysis of intelligent reflecting surface aided communication systems," *IEEE Commun. Lett.*, vol. 24, no. 11, pp. 2464-2468, Nov. 2020.

[15] A. A.-Hourani, S. Kandeepan, and S. Lardner, "Optimal LAP altitude for maximum coverage," *IEEE Wireless Commun. Lett.*, vol. 3, no. 6, pp. 569-572, Dec. 2014.

[16] L. Yang, F. Meng, J. Zhang, M. O. Hasna, and M. D. Renzo, "On the performance of RIS-assisted dual-hop UAV communication systems," *IEEE Trans. Veh. Technol.*, vol. 69, no. 9, pp. 10385-10390, Sep. 2020.

[17] M. Di Renzo *et al.* "Smart radio environments empowered by reconfigurable intelligent surfaces: How it works, state of research, and the road ahead," *IEEE J. Sel. Areas Commun.*, vol. 38, no. 11, pp. 2450-2525, Nov. 2020.

[18] U. Singh, S. Solanki, D. S. Gurjar, P. K. Upadhyay and D. B. da Costa, "Wireless power transfer in two-way AF relaying with maximal-ratio combining under Nakagami-*m* fading," in *2018 Int. Wireless Commun. Mob. Comp. Conf. (IWCMC)*, Limassol, Cyprus, Aug. 2018, pp. 169-173.

[19] T. V. Chien, L. T. Tu, S. Chatzinotas, and B. Ottersten, "Coverage probability and ergodic capacity of intelligent reflecting surface-enhanced communication systems," *IEEE Commun. Lett.*, vol. 25, no. 1, pp. 69-73, Jan. 2021.